AD-A064 447 AUBURN UNIV ALA ENGINEERING EXPERIMENT STATION F/G 20/11
INVESTIGATION OF PRINCIPAL STRAINS BY HOLOGRAPHIC MEASUREMENTS --ETC(U)
AUG 78 W H LANE, W F RANSON, W F SWINSON DAAK40-77-C-0002
UNCLASSIFIED AU-ME-AMC-0002 NL

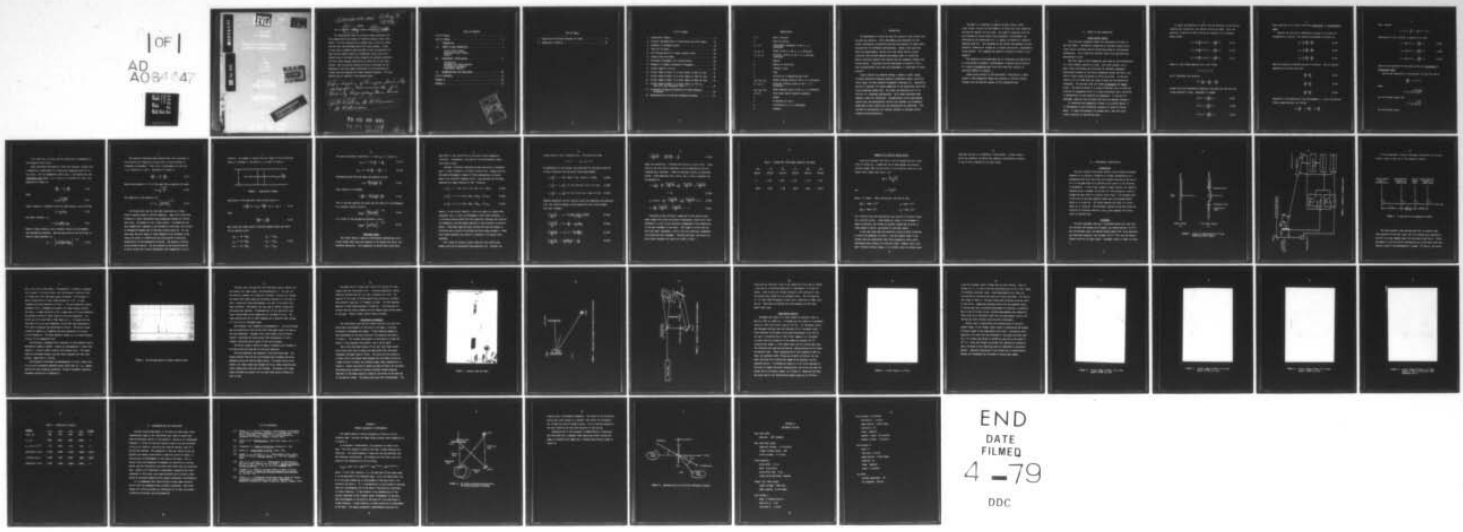

END
DATE FILMED
4-79
DDC

(14) AU-ME-AMC-0002 (11) Aug 78

(12) 49 p.

(9) PREFACE (15)

This is the final report on contract AMC DAAK40-77-C-0002 ME

The investigation under this contract sought techniques that were nondestructive and capable of revealing residual stress information. The first approach was to thermal shock a point on a model and with real time holography watch the fringe response. Liquid air was used to thermally shock the model as well as electrical hot spots but the unknown function of temperature versus time of the thermal pulse at the model surface rendered this approach unsuitable. Also the fringe response observed was not definitive of the stress applied. Next an acoustic impulse was given to the model but the magnitude of the pulse seemed insufficient to allow monitoring of fringes that were expected with double exposed holography. The final approach used is detailed in the attached report.

(6) Investigation of Principal Strains By Holographic Measurements of a Radially Propagating Wave Front.

per p2

(10) H. H. Lane, H. F. Ranson
H. F. Swinson

TABLE OF CONTENTS

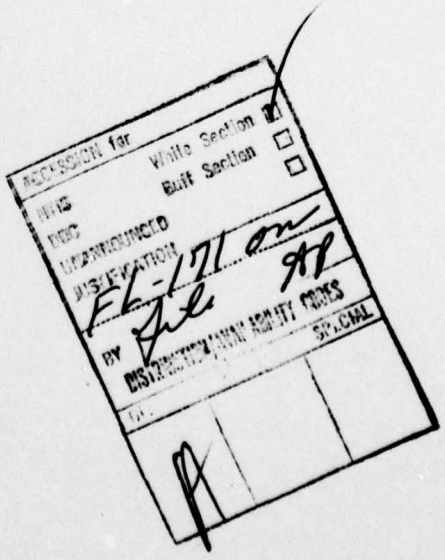

LIST OF TABLES

LIST OF FIGURES

NOMENCLATURE

λ, G	Lame's constants
e	Cubic dilitation
u, v, w	Displacement components in the x, y, z directions
ε_x, ε_y, ε_z	Normal strains in the x, y, z directions
ε_1, ε_2, ε_3	Principal strains in the 1, 2, 3 principal directions
ρ	Density
E	Modulus of elasticity
μ	Poisson's ratio
t	Time
C	Velocity of a propagating wave front
σ_{xx}, σ_{yy}, σ_{zz}	Normal stresses acting in the x, y, z directions
σ_1, σ_2, σ_3	Principal stresses acting in the 1, 2, 3 directions.
σ_{xy}, σ_{yz}, σ_{xz}	Shear stresses acting in the x, y, z directions
ℓ, m, n	Third order elastic material constants
L	Length
ψ	A function of x and t
ϕ	A function of x, y, z coordinates
a	Constant

I. INTRODUCTION

The measurement of stress has been the subject of many studies over the past two centuries. Early experiments were concerned with the elastic deformations of materials and the distributions of loads within the materials for different configurations. Based on the resulting theory and measurements, designs utilizing safety factors yielded structures that assured adequate performance under all conditions. Modern technology requires that designs now have adequate strength with minimum weight. Concurrent with the development of materials with a high strength/weight ratio were the advancements in techniques of stress analysis.

Stress analysis has advanced through a number of useful stages including destructive testing, optically transparent models, sensitive strain gages, and more recently holographic techniques [1]. Destructive testing is important for actual comparison to the predictions found from using transparent models [2]. The latter two techniques are for an analysis of a completed configuration. While these techniques seem complete, there are limitations. Non-destructive strain gage methods require that the configuration initially be unloaded, and holographic techniques to date require that the configuration be undeformed. This provides no consideration for residual stresses or permanent strain produced during manufacture.

The need for a technique to measure residual stress, and/or actual stress, without the requirement of a before and after comparison, provided the impetus for this study. The specific technique involving wave propagation versus stress using holographic interferometry was stimulated by the observation of W. F. Ranson's hologram of a centrally impacted plate [1]. This hologram did not exhibit the expected circular concentric formation of fringes but a slightly noncircular, nonconcentric fringe pattern. This prompted the specific direction of thrust in this research.

The objective of the experiment was to investigate the possibility of using dynamic holographic interferometry to measure the ellipticity of a radially propagating wave front and relate this directly to principal strains or stresses.

Before going directly to the experimental investigation, a background in wave propagation theory was necessary to provide valuable insights into the physical aspects of the propagating wave.

II. THEORY OF WAVE PROPAGATION

Linear Elastic Theory

The first wave propagation theory was formulated by Poisson in the late 1820's. The material chosen was an isotropic elastic solid. Linear elastic relations used by Poisson were based on infinitesimal deformations. This allowed the nonlinear terms to be negligible and approximated as zero.

The first ideas of wave propagation were based on the consideration of a force suddenly applied to a body. Just after contact, only a small region surrounding the force would be deformed; subsequent deformations produced by the force propoagated through the body in the form of elastic waves [3] moving at finite velocities. In the derivation it will be shown that two types of waves can be produced and propagated. The two wave types are termed dilitational and distortional. The particle motion in a plane dilitational wave is along the direction of propagation while in a plane distrotional wave, the motion is perpendicular to the direction of propagation. If the solid is unbounded, these are the only waves that can be propagated through it.

In discussing the propagation of waves in an elastic medium, it is advantageous to use differential equations in terms of displacements. If these displacements are assumed small, then the linear elastic equations of equilibrium apply.

To obtain the equations of motion from the equations of equilibrium, assuming body forces zero, the inertial forces are added. Thus, the equations of motion for small strains and rotations in an isotropic medium become

$$(\lambda + G)\frac{\partial e}{\partial x} + G\,\nabla^2 u - \rho\frac{\partial^2 u}{\partial t^2} = 0 \qquad (2.1a)$$

$$(\lambda + G)\frac{\partial e}{\partial y} + G\,\nabla^2 v - \rho\frac{\partial^2 v}{\partial t^2} = 0 \qquad (2.1b)$$

$$(\lambda + G)\frac{\partial e}{\partial z} + G\,\nabla^2 w - \rho\frac{\partial^2 w}{\partial t^2} = 0 \qquad (2.1c)$$

where e is the volume expansion for a unit volume

$$e = \varepsilon_x + \varepsilon_y + \varepsilon_z$$

and ∇^2 represents the operation

$$\nabla^2 = \frac{\partial^2}{\partial x^2} + \frac{\partial^2}{\partial y^2} + \frac{\partial^2}{\partial z^2}$$

Assume first that deformation produced by the waves are such that the volume expansion is zero. Equations 2.1 become

$$G\,\nabla^2 u - \rho\frac{\partial^2 u}{\partial t^2} = 0 \qquad (2.2a)$$

$$G\,\nabla^2 v - \rho\frac{\partial^2 v}{\partial t^2} = 0 \qquad (2.2b)$$

$$G\,\nabla^2 w - \rho\frac{\partial^2 w}{\partial t^2} = 0 \qquad (2.2c)$$

These equations are for waves called the distortional, or equivoluminal waves.

Consider now the case of deformation produced by the waves not accompanied by rotation. The rotation-displacement relations are

$$\omega_x = \frac{1}{2}\left(\frac{\partial w}{\partial y} - \frac{\partial v}{\partial z}\right) \tag{2.3a}$$

$$\omega_y = \frac{1}{2}\left(\frac{\partial u}{\partial z} - \frac{\partial w}{\partial x}\right) \tag{2.3b}$$

$$\omega_z = \frac{1}{2}\left(\frac{\partial v}{\partial x} - \frac{\partial u}{\partial y}\right) \tag{2.3c}$$

where the subscript indicates the axis of rotation. With no rotation equations 2.3 are zero and yield

$$\frac{\partial w}{\partial y} = \frac{\partial v}{\partial z} \tag{2.4a}$$

$$\frac{\partial u}{\partial y} = \frac{\partial v}{\partial x} \tag{2.4b}$$

$$\frac{\partial w}{\partial x} = \frac{\partial u}{\partial z} \tag{2.4c}$$

Equations 2.4 are satisfied if the displacement u, v, and w are derived from a single function ϕ as follows

$$u = \frac{\partial \phi}{\partial x}, \quad v = \frac{\partial \phi}{\partial y}, \quad w = \frac{\partial \phi}{\partial z}$$

Then e becomes

$$e = \nabla^2 \phi, \quad \frac{\partial e}{\partial x} = \frac{\partial}{\partial x} \nabla^2 \phi = \nabla^2 u$$

Substitution of this relation in equation 2.2 yields

$$(\lambda + 2G) \nabla^2 u - \rho \frac{\partial^2 u}{\partial t^2} = 0 \qquad (2.5a)$$

$$(\lambda + 2G) \nabla^2 v - \rho \frac{\partial^2 v}{\partial t^2} = 0 \qquad (2.5b)$$

$$(\lambda + 2G) \nabla^2 w - \rho \frac{\partial^2 w}{\partial t^2} = 0 \qquad (2.5c)$$

These are the equations for the waves called the irrotational or dilatational waves.

Notice that equations 2.2 and equations 2.5 have the form of

$$\frac{\partial^2 \psi}{\partial t^2} = a^2 \nabla^2 \psi$$

where

$$a = C_1 = \sqrt{\frac{\lambda + 2G}{\rho}}$$

for dilitational waves, and

$$a = C_2 = \sqrt{\frac{G}{\rho}}$$

for dilitational waves.

As it turns out, C_1 and C_2 are the velocities of propagation of the respective wave fronts.

Again considering the material linear and isotropic, without loss of generality, assume there is a plane wave propagating parallel to the x-axis. Let its propagation velocity be C. Considering only the longitudinal wave where v = w = 0 and u is a function of x only, the equations 2.5 reduce to

$$\frac{\partial^2 u}{\partial t^2} = C_L^2 \frac{\partial^2 u}{\partial x^2} \tag{2.6}$$

where

$$C_L = \sqrt{\frac{\lambda + 2G}{\rho}} \tag{2.7}$$

Lame's constant G, sometimes called the shear modulus, can be written

$$G = \frac{E}{2(1 + \mu)} \tag{2.8}$$

and Lame's constant λ is

$$\lambda = \frac{\mu E}{(1 + \mu)(1 - 2\mu)} \tag{2.9}$$

where E, Young's Modulus, and μ, Poisson's Ratio, are the commonly used engineering constants. Then the wave velocity can be written in terms of these constants, or

$$C_L = \left[\frac{E(1 - \mu)}{(1 + \mu)(1 - 2\mu)\rho}\right]^{1/2} \tag{2.10}$$

Now consider transverse waves assuming that the x-direction is the direction of propagation and the y-axis is the direction of transverse displacement. Then u and w displacements are zero and v is a function of x and t. Equations 2.4 reduce to

$$\frac{\partial^2 v}{\partial t^2} = C_T^2 \frac{\partial^2 v}{\partial x^2} \tag{2.11}$$

Notice that equation 2.11 is of the same form as equation 2.6 where

$$C_T = \sqrt{\frac{G}{\rho}} \tag{2.12}$$

and comparing it with equation 2.10

$$C_T = C_L \left[\frac{1 - 2\mu}{2(1 - \mu)}\right]^{1/2} \tag{2.13}$$

The formulations thus far have been restricted to a linear elastic isotropic body of infinite dimension. Lamb (1917) solved the problem of a plane longitudinal wave propagating through an infinite thin plate. The medium is still linear elastic. He showed that for wave lengths small compared to the thickness of the plate, the velocity of propagation becomes that of Rayleigh surface waves [4]. For the case where the wave length is large compared to the thickness of the plate, the stress is uniform over any cross-section of the plate perpendicular to the propagation direction. The equation of motion can be derived directly. Let the surfaces of the plate be parallel to the xy plane with a plane longitudinal wave propagating in the x-

direction. An element is chosen with unit length in the y-direction, width Δx, thickness d, and density ρ, as shown in Figure 1.

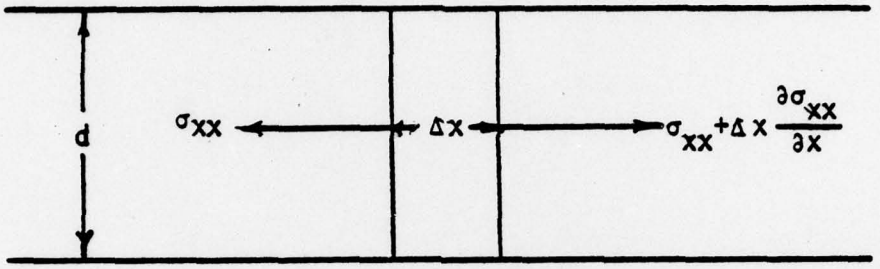

FIGURE 1. Longitudinal Element

Application of the equation of equilibrium results in

$$\rho d \frac{\partial^2 u}{\partial t^2} \Delta x = (\sigma_{xx} + \frac{\partial \sigma_{xx}}{\partial x} \Delta x)\, d - \sigma_{xx}\, d \qquad (2.14)$$

Thus,

$$\frac{\partial \sigma_{xx}}{\partial x} = \rho \frac{\partial^2 u}{\partial t^2} \qquad (2.15)$$

Now, using the linear elastic relations between stress and strain for an isotropic solid

$$\begin{aligned} \sigma_{xx} &= \lambda e + 2G\epsilon_x & \sigma_{xy} &= G\epsilon_{xy} \\ \sigma_{yy} &= \lambda e + 2G\epsilon_y & \sigma_{yz} &= G\epsilon_{yz} \\ \sigma_{zz} &= \lambda e + 2G\epsilon_z & \sigma_{zx} &= G\epsilon_{zy} \end{aligned} \qquad (2.16)$$

and applying boundary conditions, $v = 0$ and $\sigma_{zz} = 0$, results in

$$\sigma_{xx} = (\lambda + 2G) \frac{\partial u}{\partial x} + \lambda \frac{\partial w}{\partial z} \tag{2.17a}$$

$$\sigma_{zz} = (\lambda + 2G) \frac{\partial w}{\partial z} + \lambda \frac{\partial u}{\partial x} = 0 \tag{2.17b}$$

Eliminating dw/dz from the above two equations yields

$$\sigma_{xx} = \frac{4G\ (\lambda + G)}{(\lambda + 2G)} \frac{\partial u}{\partial x} \tag{2.18}$$

Thus, equation 2.15 becomes

$$\rho \frac{\partial^2 u}{\partial t^2} = \frac{4G\ (\lambda + G)}{(\lambda + 2G)} \frac{\partial^2 u}{\partial x^2} \tag{2.19}$$

This is the wave equation and shows that the waves will be propagated at a constant velocity given by

$$C_{LAMB} = \left[\frac{4G\ (\lambda + G)}{\rho(\lambda + G)}\right]^{1/2} \tag{2.20}$$

or in terms of the engineering constants, E and μ,

$$C_{LAMB} = \left[\frac{E}{\rho(1 - \mu^2)}\right]^{1/2} \tag{2.21}$$

Nonlinear Theory

The linear theory is based on infinitesimal deformations which allows second order terms and products to be assumed very small, and therefore negligible. This assumption of second order terms being

negligible is very restrictive in the case of wave propagation velocities. Consequently, the need for finite deformation theory (nonlinear) arises.

Consider a principal coordinate system consisting of orthogonal axes 1, 2 and 3 located in a triaxial strain field. Hughes and Kelly [5] applied Murnaghan's theory of finite deformations to elastic waves in an initially isotropic solid. They obtained the following equations for waves traveling in the 1 direction

$$\rho_o C_{11}^2 = \lambda + 2G + (2\ell + \lambda)e + (4m + 4\lambda + 10G)\varepsilon_1 \qquad (2.22a)$$

$$\rho_o C_{12}^2 = G + (\lambda + m)e + 4G\varepsilon_1 + 2G\varepsilon_2 - 1/2\, n\varepsilon_3 \qquad (2.22b)$$

$$\rho_o C_{13}^2 = G + (\lambda + m)e + 4G\varepsilon_1 + 2G\varepsilon_2 - 1/2\, n\varepsilon_3 \qquad (2.22c)$$

where ρ_o is the initial density, λ and G are Lame's or second order constants, and ℓ, m and n are Murnaghan's third order constants. C is the wave velocity where the first subscript indicates the direction of propagation, and the second subscript is the direction of particle motion. From these equations Egle and Bray [6] used the change in velocities due to strain to evaluate the third order constants. These third order constants are similar to Truesdell's [7] second order constants.

For a state of uniaxial stress, there are five unique wave speeds which may be determined from equations 2.22. Consider the

stress acting in the 1 direction only. The strains are then

$$\varepsilon_1 = \varepsilon \qquad \varepsilon_2 = \varepsilon_3 = -\mu\varepsilon$$

By permutation of the indices, the velocities for the waves traveling in the 2 direction with the strain field above become

$$\rho_o C_{22}^2 = \lambda + 2G + [2\ell(1 - 2\mu) - 4\mu(m + \lambda + 2G)]\varepsilon \qquad (2.23a)$$

$$\rho_o C_{21}^2 = \rho_o C_{31}^2 = G + [(\lambda + 2G + m)(1 - 2\mu) + 1/2\ m\mu]\varepsilon \qquad (2.23b)$$

$$\rho_o C_{23}^2 = \rho_o C_{32}^2 = G + [(\lambda + m)(1 - 2\mu) - 6\mu G - 1/2\ n]\varepsilon \qquad (2.23c)$$

Reducing equations 2.22 for uniaxial strain and combining with equations 2.23, the relative changes in wave speed with axial strain become (for small changes)

$$\frac{d\ C_{11}/C_{11}^\circ}{d\varepsilon} = 2 + \frac{G + 2m + \mu G(1 + 2\ell/\lambda)}{\lambda + 2G} \qquad (2.24a)$$

$$\frac{d\ C_{12}/C_{12}^\circ}{d\varepsilon} = 2 + \frac{\mu n}{4G} + \frac{m}{2(\lambda + G)} \qquad (2.24b)$$

$$\frac{d\ C_{22}/C_{22}^\circ}{d\varepsilon} = -2\mu\ \left(1 + \frac{m - G\ell/\lambda}{\lambda + 2G}\right) \qquad (2.24c)$$

$$\frac{d\ C_{21}/C_{21}^\circ}{d\varepsilon} = \frac{\lambda + 2G + m}{2(\lambda + G)} + \frac{\mu n}{4G} \qquad (2.24d)$$

$$\frac{d\, C_{23}/C_{23}^{\circ}}{d\varepsilon} = \frac{(m - 2\lambda)}{2(\lambda + G)} - \frac{n}{4G} \qquad (2.24e)$$

Where the superscript ∘ indicates the velocity at zero strain. These terms on the left side of equations 2.24 are sometimes called the acoustoelastic constants. These are obtained directly by experimentation. Using equations 2.24 c and e, the ℓ, m and n constants can be expressed as

$$\ell = \frac{\lambda}{1-2\mu}\left[\frac{1-\mu}{\mu}\frac{d\, C_{22}/C_{22}^{\circ}}{d\varepsilon} + \frac{2}{1+\mu}\frac{d\, C_{21}/C_{21}^{\circ}}{d\varepsilon} + \mu\frac{d\, C_{23}/C_{23}^{\circ}}{d\varepsilon}\right] + 2\mu \qquad (2.25a)$$

$$m = 2(\lambda+G)\left[\frac{\mu}{1-\mu}\frac{d\, C_{23}/C_{23}^{\circ}}{d\varepsilon} + \frac{1}{1+\mu}\frac{d\, C_{21}/C_{21}^{\circ}}{d\varepsilon}\right] + 2\mu - 1 \qquad (2.25b)$$

$$n = \frac{4G}{1+\mu}\left[\frac{d\, C_{21}/C_{21}^{\circ}}{d\varepsilon} - \frac{d\, C_{23}/C_{23}^{\circ}}{d\varepsilon}\right] - 1 - \mu \qquad (2.25c)$$

According to Egle and Bray's comparison of the relative wave speed change with strain with other investigators, these third order constants (ℓ, m and n) are relatively independent of the composition or the heat treatment of the steel. This seems to follow from the fact that Lame's constants, λ and G, are also relatively independent of alloying and heat treatment. From Egle and Bray, the second and third order constants for steel are listed in Table 1.

TABLE 1. SECOND AND THIRD ORDER CONSTANTS FOR STEEL

ρ_o	λ	G	ℓ	m	n
lbm/in^3	lbf/in^2	lbf/in^2	lbf/in^2	lbf/in^2	lbf/in^2
x 1	x 10^6	x 10^6	x 10^6	x 10^6	x 10^6
.2818	16.81	11.60	-36.0	-90.4	-103.6

Example of Δ Velocity Versus Strain

Using the constants from Table 1 with an assumed uniaxial stress field of 20,000 psi, a comparison can be made between the relative velocity change (RVC) and the strain in the direction parallel to the stress field, namely the 1-axis. Let

$$RVC \equiv \frac{C_{11} - C_{11}^{\circ}}{C_{11}^{\circ}}$$

and

$$\varepsilon = \frac{L - L^{\circ}}{L^{\circ}}$$

where L is length. After calculations, the results show

$$RVC_1 = -1680 \times 10^{-6} \qquad \varepsilon_1 = 666 \times 10^{-6}$$

$$RVC_2 = +560 \times 10^{-6} \qquad \varepsilon_2 = -222 \times 10^{-6}$$

This indicates that the longitudinal wave velocity is actually slower for a positive strain. Since 20,000 psi stress is not uncommon in modern structures, this effect of velocity change due to strain is large enough to warrant application of nonlinear theory.

It has been shown that the velocities along principal directions of strain are dependent on strain. From the example shown it was evident that the longitudinal wave front propagating from a point disturbance would produce an elliptical shape. However, due to the small relative velocity change, it is unlikely that this effect would

have been noticed in a holographic fringe pattern. Further investigation was necessary to explain the seemingly contradictory evidence of the elliptic hologram [1] and wave theory.

III. EXPERIMENTAL INVESTIGATION

Introduction

The basic problem involved was taking a double exposure hologram (Appendix A) to achieve a formation of fringes representative of a propagating wave front and relate the distance traveled by the wave in 15 μs to the magnitude of an applied elastic strain in the direction of propagation. A thin plate, loaded in simple tension, was centrally impacted using a Crossman .22 caliber air rifle producing a radially propagating wave front in a biaxial strain field. The hologram taken of the side of the plate opposite impact was first exposed before impact as in Figure 2a. The second exposure was taken 15 μs after impact as in Figure 2b. The distances traveled by the wave along the direction of principal strains ε_1 and ε_2 were compared for various levels of applied load.

Equipment

The basic equipment used was a Q-switched pulsed ruby laser [8], two Textronix 549 storage oscilloscopes, one Spectra-Physics 15 milliwatt Helium-Neon laser, one Hewlett Packard, model 214A pulse generator, two photodiode detectors, one Crossman .22 air rifle, and one Hewlett Packard 0-90 volt DC power supply. Equipment layout is shown in Figure 3.

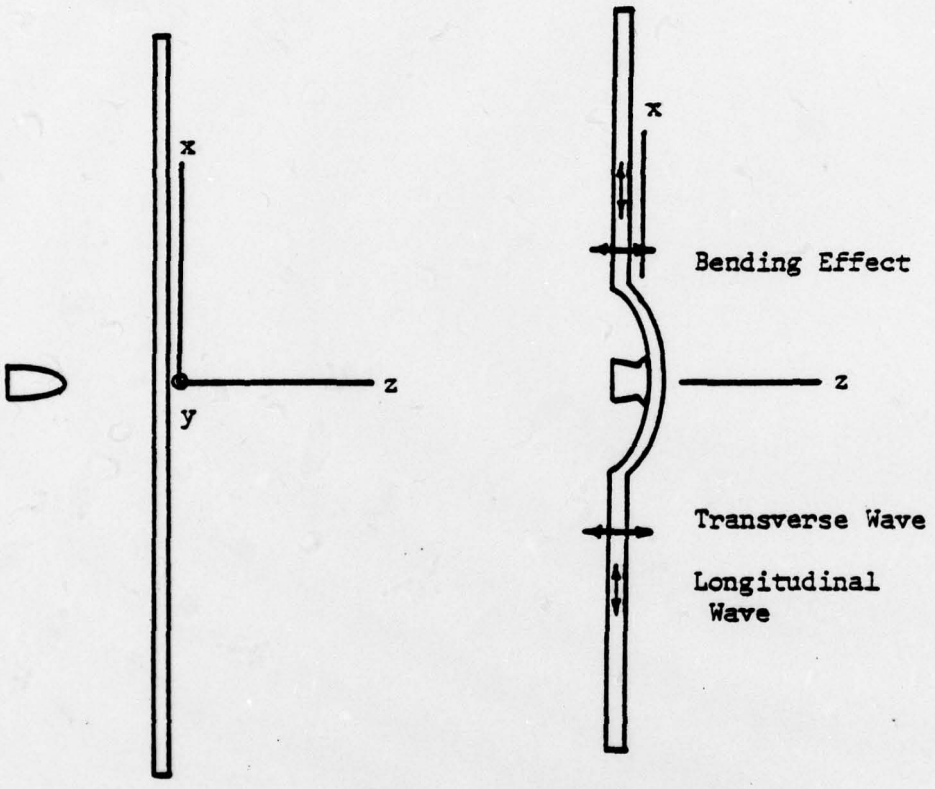

Before Impact
(a)

15 μs After Impact
(b)

FIGURE 2. Pictorial Representation of Plate Before and After Impact

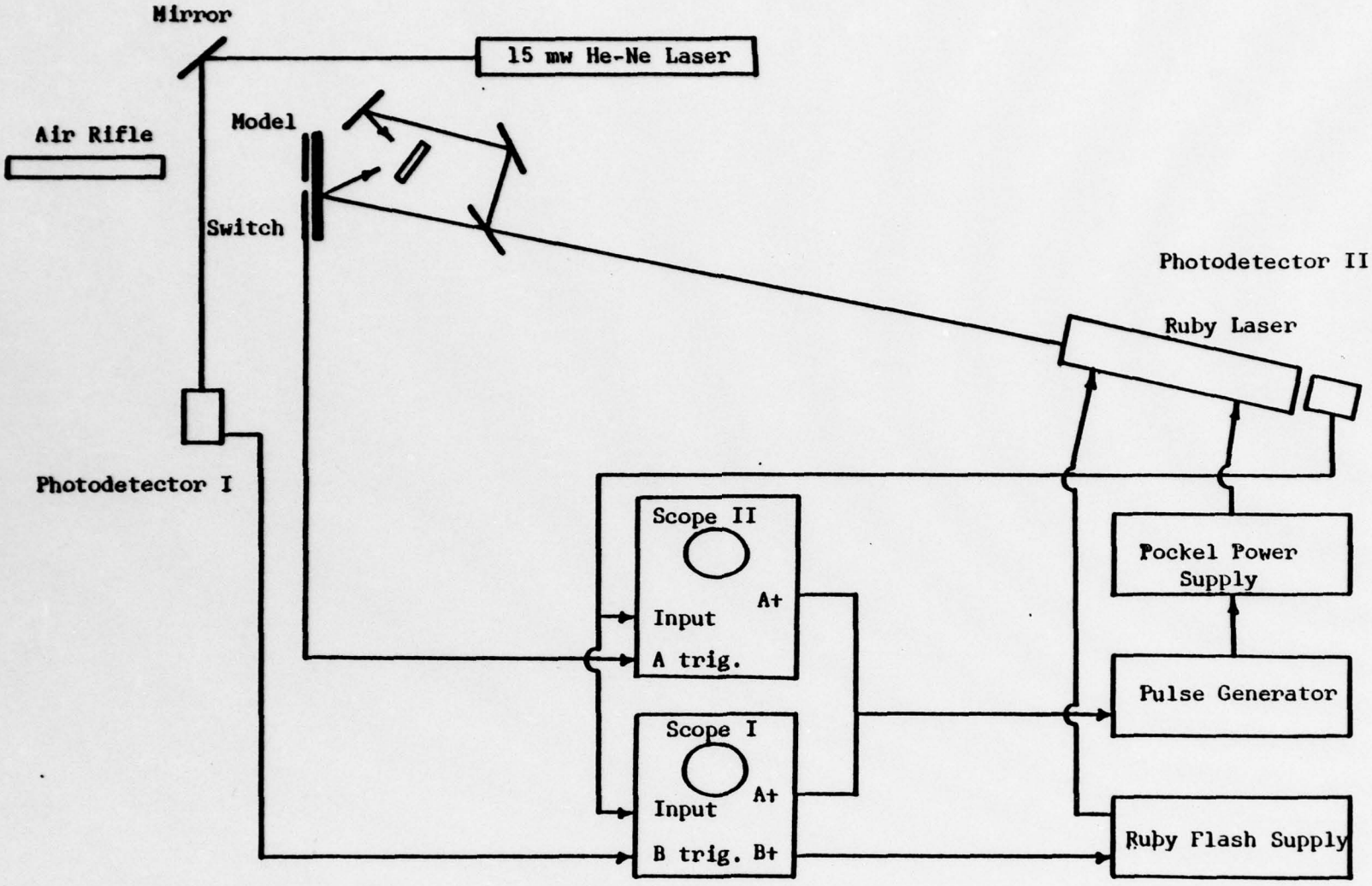

FIGURE 3. Schematic of Equipment Layout

In this experiment, timing of equipment interactions was critical. Figure 4 shows a time plot of the sequence of events.

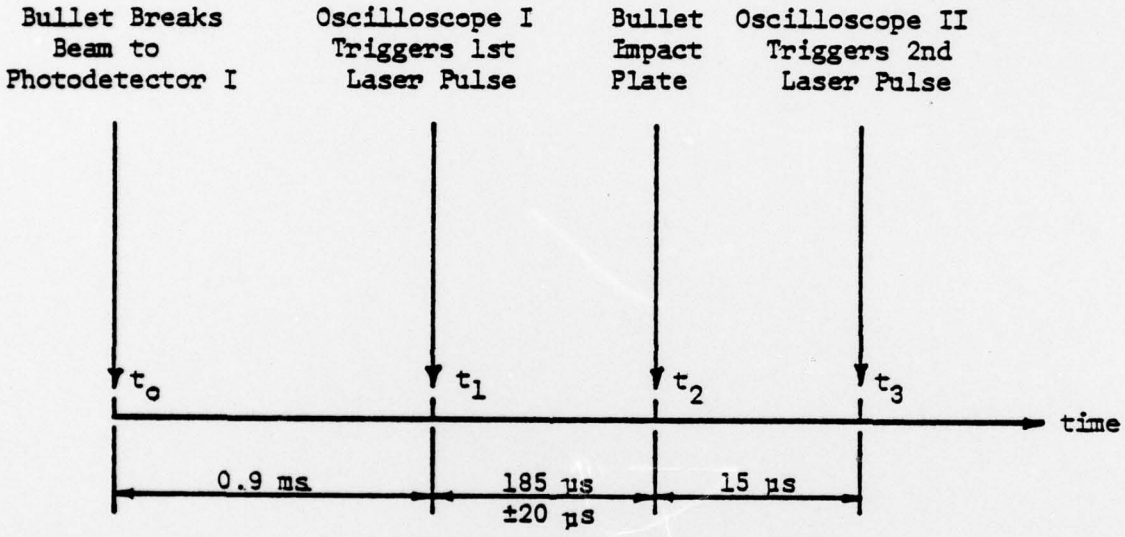

FIGURE 4. A Time Plot of the Sequence of Events

The three essential time spacings were the 1 ms optical pump time required for the ruby laser, the 70 µs minimum pulse separation, and the 15 µs span between impact and the second laser pulse. Timing was begun at t_o by the bullet interrupting the 15 milliwatt laser beam causing a gate in the photodetector I output. At time t_o, the bullet

was 1.2 ms $\pm$ 20 μs from impact. Photodetector I internally triggered oscilloscope I initiating trace B and simultaneously sending B+ gate to trigger the flash lamp power supply discharge. Oscilloscope I in mode B intensified by A had A sweep delayed by .9 ms. A+ gate triggered the pulse generator at time t_1. The pulse generator output, delayed by 15 μs, triggered the pockels cell power supply; pulsing the laser. A sweep lasted 50 μs for a sweep rate of 5 μs/cm preventing any possible overlap at input signals to the pulse generator. The bullet was still about 200 μs from impact at t_1. To assure that the time span of t_0 to t_2 was repeatable, the bullets were undersized to 0.21" and air pressure was maintained at 150 psi. The bullet closed a switch at impact t_2, triggering the pulse generator via A+ gate of oscilloscope II. The pulse generator output at t_3 is again delayed giving a 15 μs propagation time.

Oscilloscope I, equipped with a Textronix 1A1 dual-channel plug-in, monitored A+ gates on channel 1 adding the photodetector II input from channel 2. Figure 5 shows a typical oscilloscope trace. The square waves are the gated outputs, and the spikes represent the ruby laser pulses. Sweep rate is .2 ms/cm.

Oscilloscope II monitored the photodetector II using a sweep rate of 5 μs/cm to accurately determine actual delay time, $t_3 - t_2$. Repeatability for this system was excellent. Further information regarding equipment settings are in Appendix B.

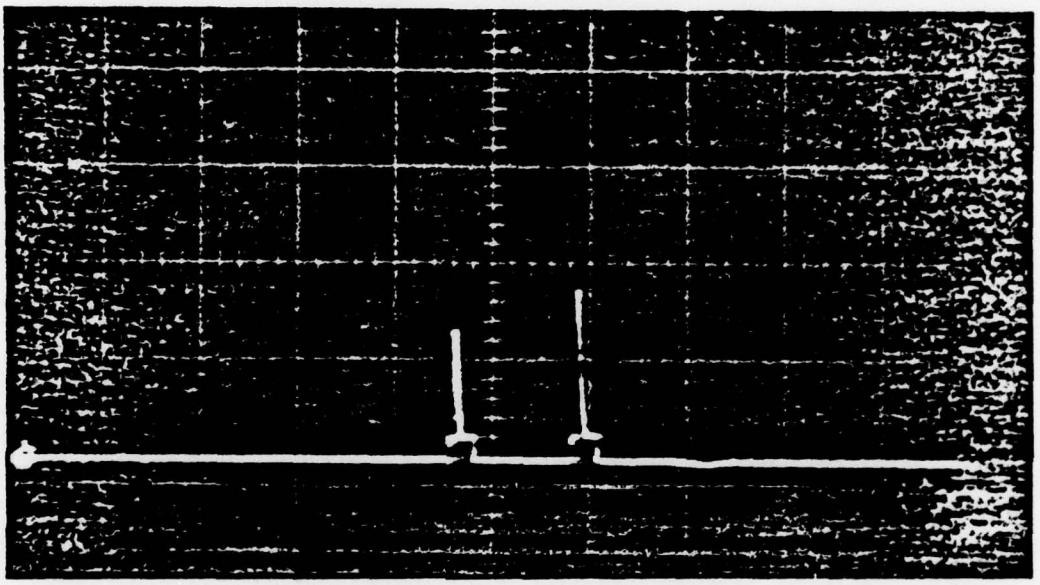

FIGURE 5. Oscilloscope Record of Double Exposure Event

The ruby laser included the flash lamp power supply, pockels cell and pockels cell power supply, and photodetector II. The ruby rod was optically pumped via a capacitor discharge, lasting 2 ms, through two xenon flash lamps supplying the energy necessary for the ruby to lase. Lasing only took place between .9 ms and 1.5 ms after flash lamp initiation. The pockels cell was used to inhibit lasing until the pulses were desired. A characteristic of this particular ruby laser limited double pulse separation to a minimum of 70 μs. The laser aperture was set at .056" diameter and a capacitor bank voltage of 1.5 kv for all holograms taken.

Oscilloscope I was triggered by photodetector I. The oscilloscope sent an output pulse first to the flash lamp power supply and then to the pulse generator. Equipped with a dual channel plug-in module, channel 1 monitored the laser pulses from photodetector II while channel 2 monitored the A+ gates of both oscilloscopes.

The bullet closed a switch on impact, triggering oscilloscope II. An output pulse was then sent to the pulse generator.

The pulse generator was operated in the pulse delay mode. The pulses received from the two oscilloscopes each triggered the pulse generator giving the desired double pulse. The output pulse to the pockels cell power supply was delayed for 15 μs, after receiving each input trigger pulse from each oscilloscope. The pockels cell power supply switched the pockels cell for each input pulse allowing the ruby to lase.

The model was an 11 gage steel plate 3.72" wide by 18" long, loaded along the longitudinal axis. A tension-compression loading frame was designed and built to load a specimen this size. The capacity of the frame is 20,000 pounds force applied by an Energy Pack hydraulic pump and 1.5" diameter cylinder. The hand operated pump has a rated output maximum of 10,000 psi. The force was calculated from the piston diameter and the pressure gage reading taken at the pump. Figure 6 shows loading frame with model.

Holographic Arrangement

The longitudinal wave has the highest velocity, and since this would cause displacements in the plane of the model, a suitable holographic arrangement was needed. Fringe formation depends on the displacement of the body along the line bisecting the angle α in Figure 7. For inplane displacement to contribute to fringe formation, it was necessary that angles θ and ψ not be equal.

Due to the high power density of the ruby laser beam, ground glass plates were used to expand the beam rather than the normal convergent divergent spatial filter. The glass was only ground on a single side so the object beam expander was also made to serve as a beam splitter to obtain the reference beam, shown schematically in Figure 8. Unless high quality lenses and beam splitters are available, the ground glass system will produce holograms without unwanted "motling" of the image caused by intensity variations of the beam due to low quality lenses. The ground glass does have disadvantages. The

FIGURE 6. Loading Frame and Model

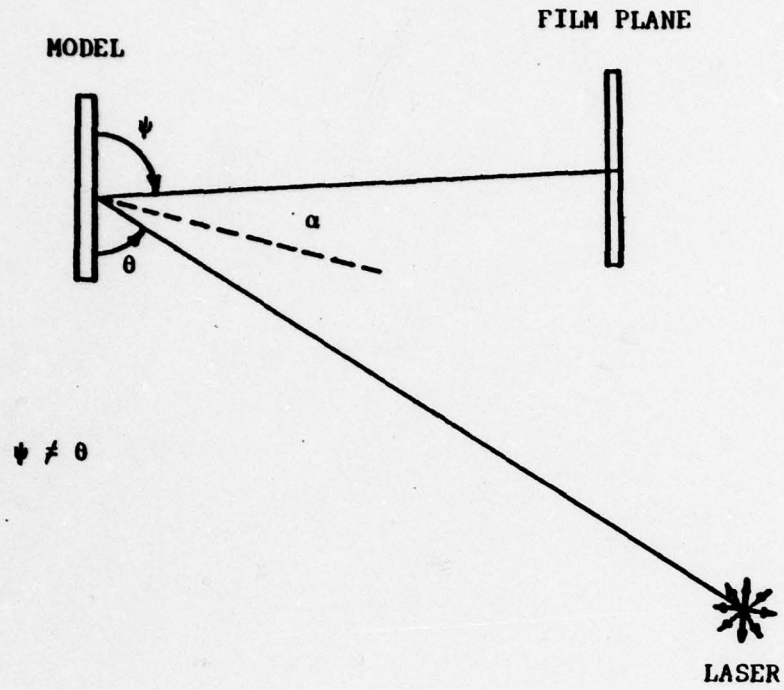

FIGURE 7. Holographic Arrangement for Measuring In-Plane Motion

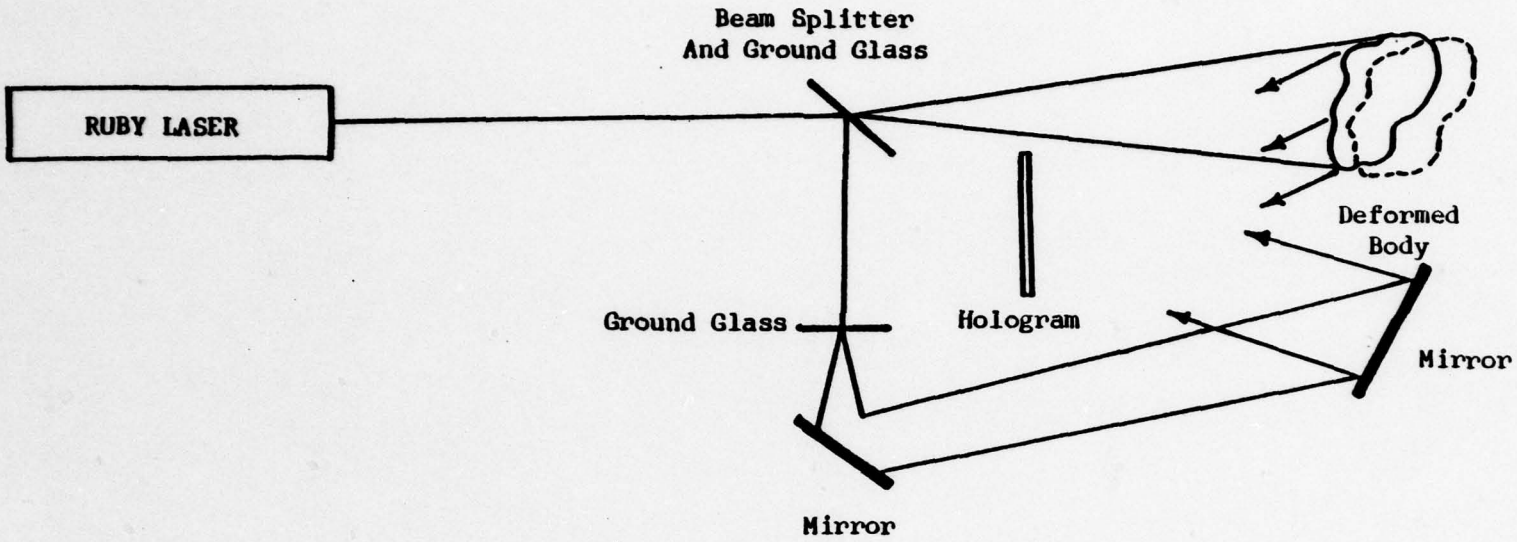

FIGURE 8. Schematic of Dynamic Holography Arrangement

glass must be relatively close to the object and film plane to prevent a very grainy illumination beam which is detrimental to fringe formation. Even at best the fringes produced by this particular laser and ground glass system are not extremely sharp. The film used was 4" x 5" Agfa 10E75 holographic plates with a resolution of 2800 lines per cm. There were no problems with over-exposure for the laser power levels used.

Experimental Results

Holograms were taken 15 μs after impact at tensional loads of 800 lb_f, 4420 lb_f, 8830 lb_f. A hologram was also taken for a permanent strain of .0015 in/in with a load of 1770 lb_f. All distances, angles and equipment settings were held constant for all holograms taken. A Nikon Nikkormat 35 mm camera using Kodak Panchromatic film, ASA 32, was used in reconstruction of the virtual images of all holograms. To assure that any distorsion of the image was constant for all reconstructed images, a rigid camera mount and film holder were used. The reconstruction beam was provided by a Spectra-Physics 50 milliwatt helium-neon laser. After reconstruction of the hologram at 4420 lb_f load, the outermost radial fringe was slightly elliptical, but the major and minor axis orientations seemed to be reversed from the expected results. A hologram was taken of a 3.8" circle centered at the point of impact and after reconstruction, the circle had been distorted into an elliptical shape, as in Figure 9. Measuring the major and minor axes on the reconstructed images proved to be difficult

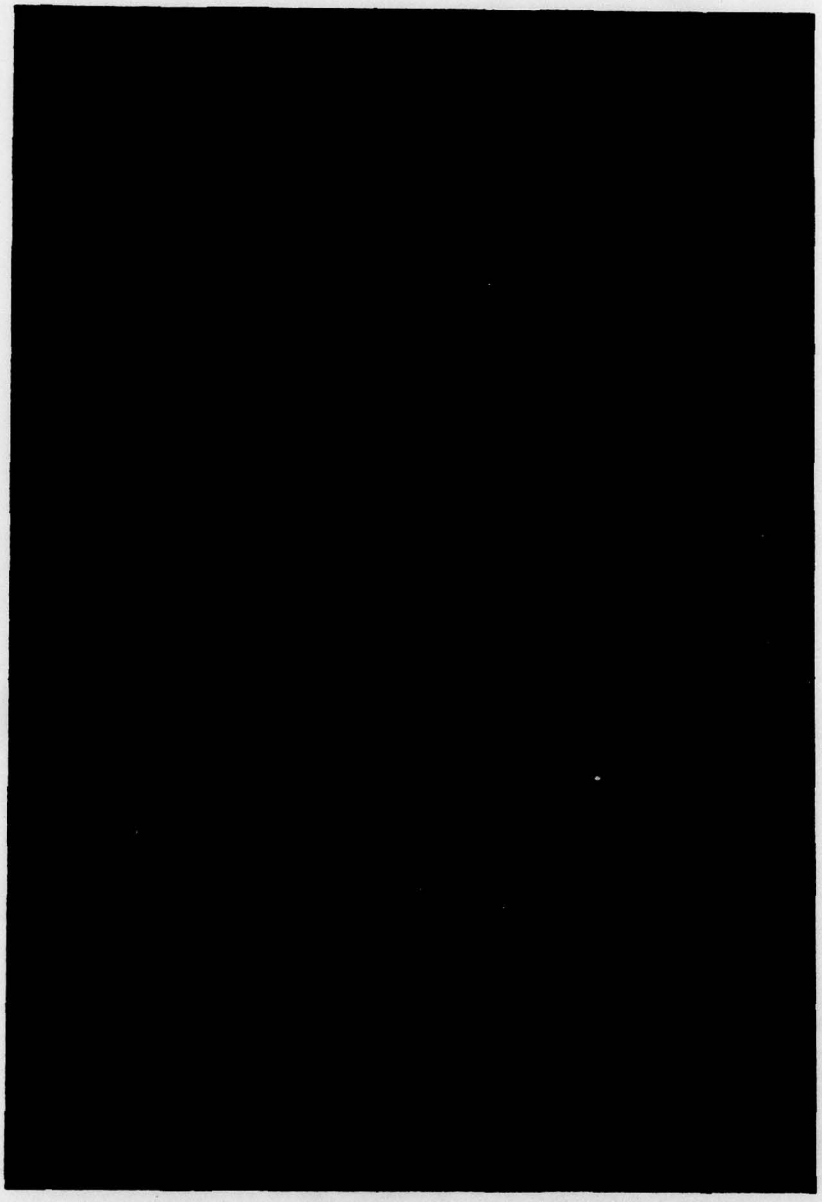

FIGURE 9. Virtual Image of a Circle

since the outermost radial fringes were not well defined. Shown in Figures 10, 11, 12, and 13 are the reconstructions of the virtual images for different tensional loads. Rough measurements were taken and calculations of the major and minor axis ratios were made. The results are listed in Table 2. The wave fronts were corrected using the ratio of the circle. Camparing corrected ratios with the expected ratios, it can be seen that an accurate measurement of distances is essential. Due to lack of fringe clarity, accurate measurements were impossible. There could be no conclusion drawn from the experimental results concerning the strain (stress) wave velocity relationship.

Optics, both in construction and reconstruction of the holographic image, is the largest single factor in determining the pseudo-elliptical shape of the longitudinal wave front. Calculation using equations 2.21a show that the difference in the major and minor axes for a 15 μs delay and stress of 20,000 psi would be on the order of 10^{-3} in. Since the fringes are neither well defined nor concentric, then a distance of this magnitude would be impossible to accurately measure. Apparent distortions of the fringes due to reconstruction effects far overshadow the influence of varying wave speeds.

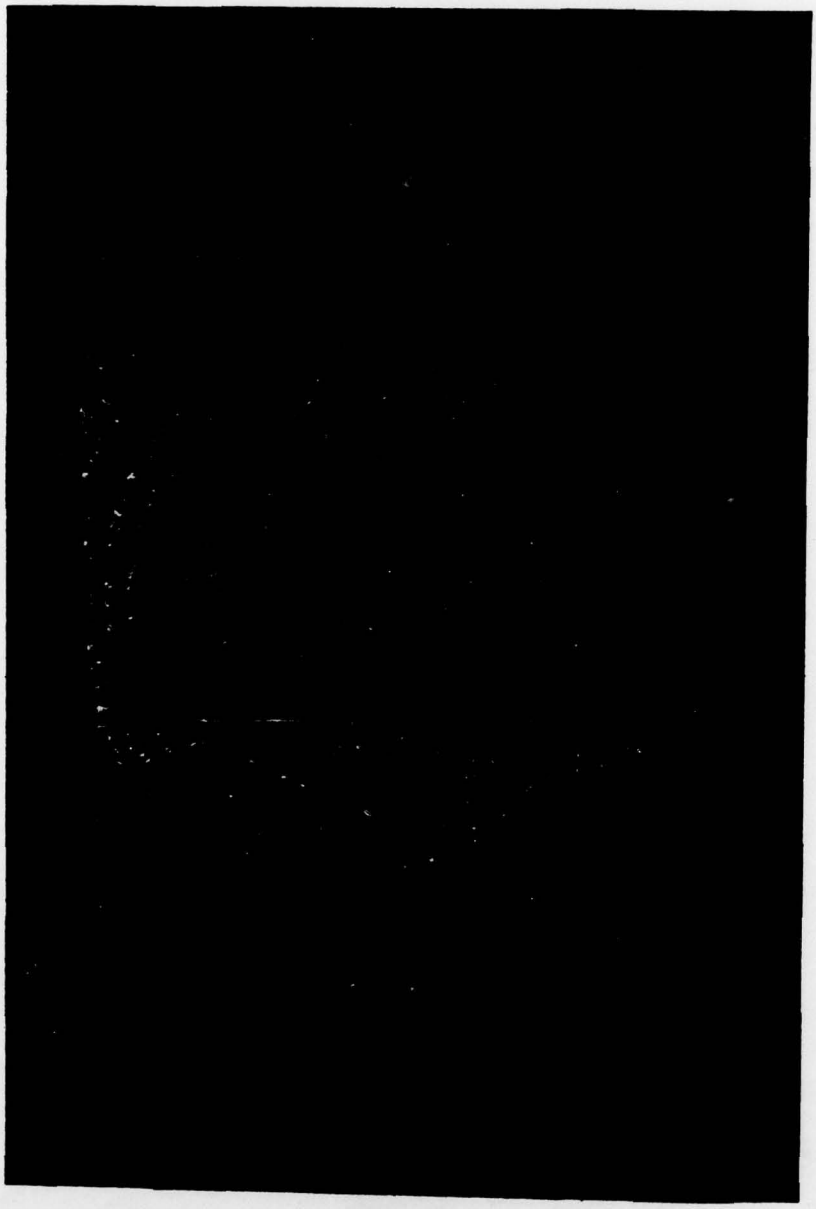

FIGURE 10. Virtual Image of Model 15 μs after Impact at 880 lb_f Load

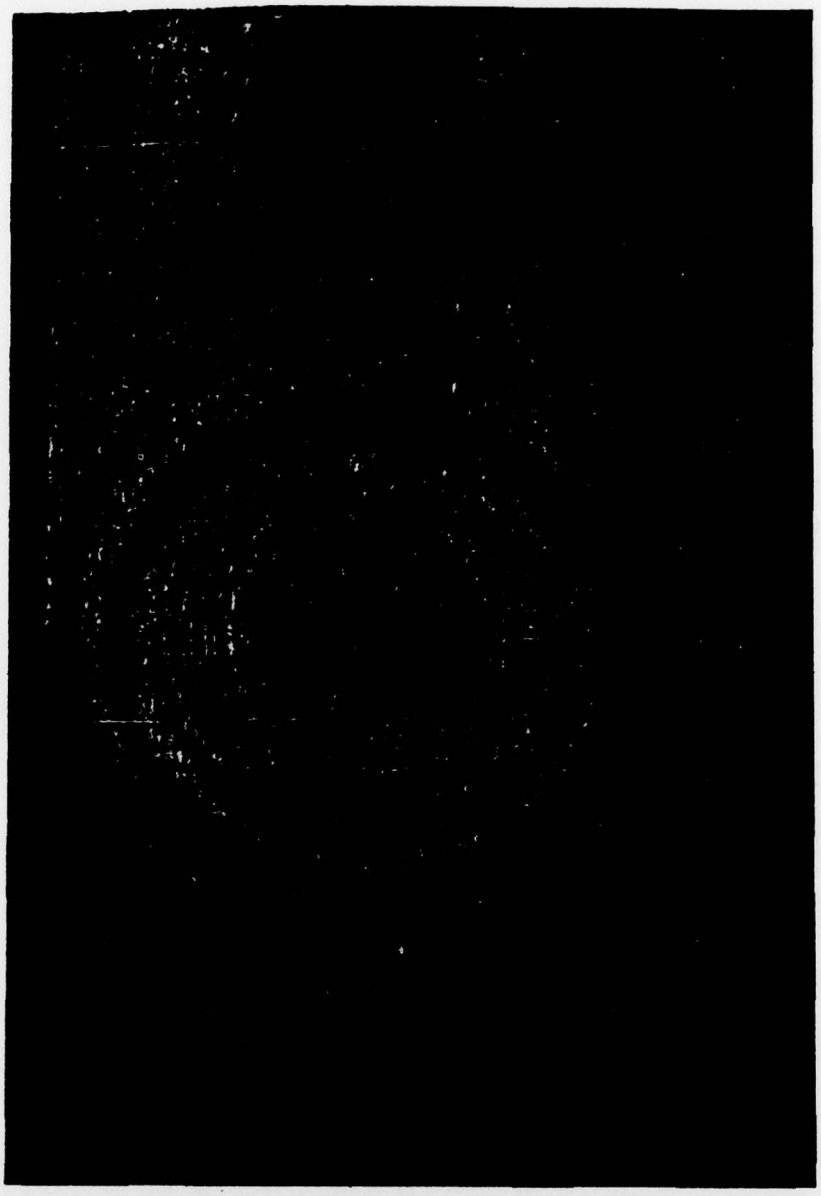

FIGURE 11. Virtual Image of Model 15 μs After Impact at 4420 lb_f Load

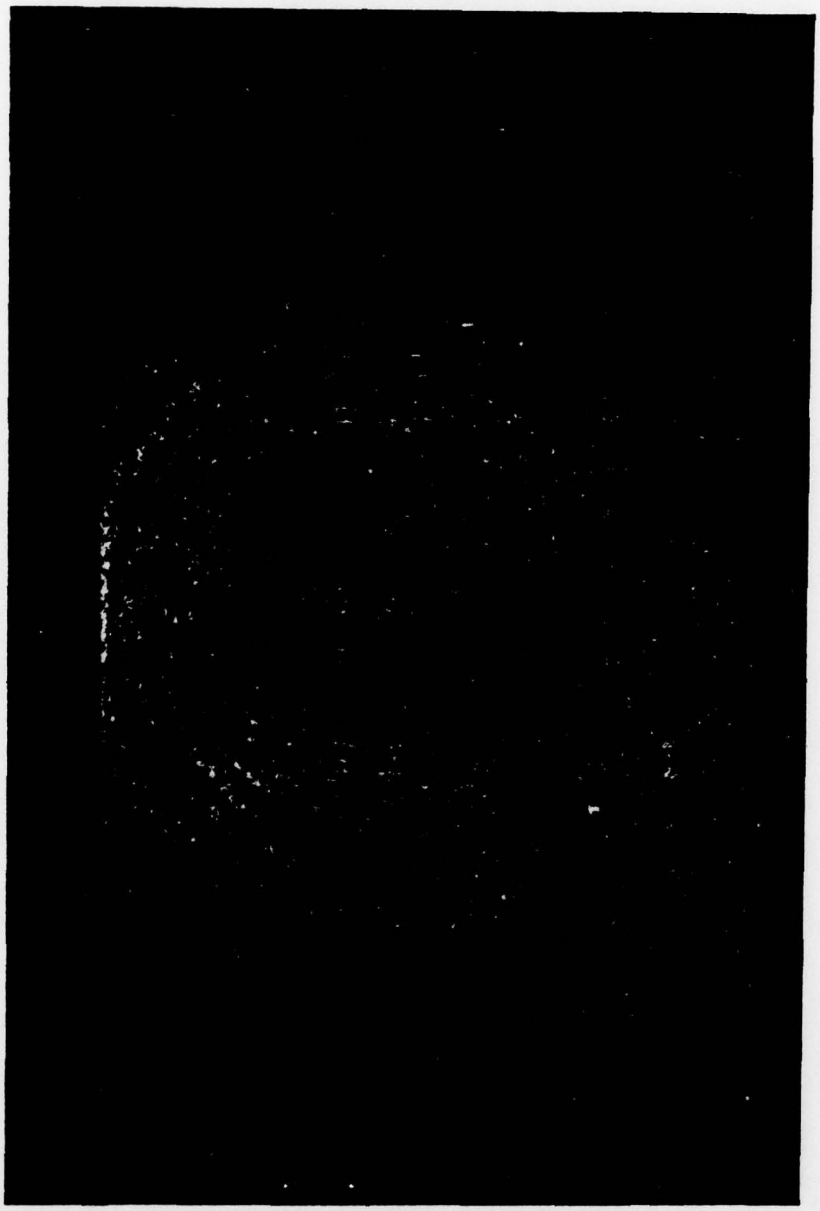

FIGURE 12. Virtual Image of Model 15 μs After Impact at 8835 lb_f Load

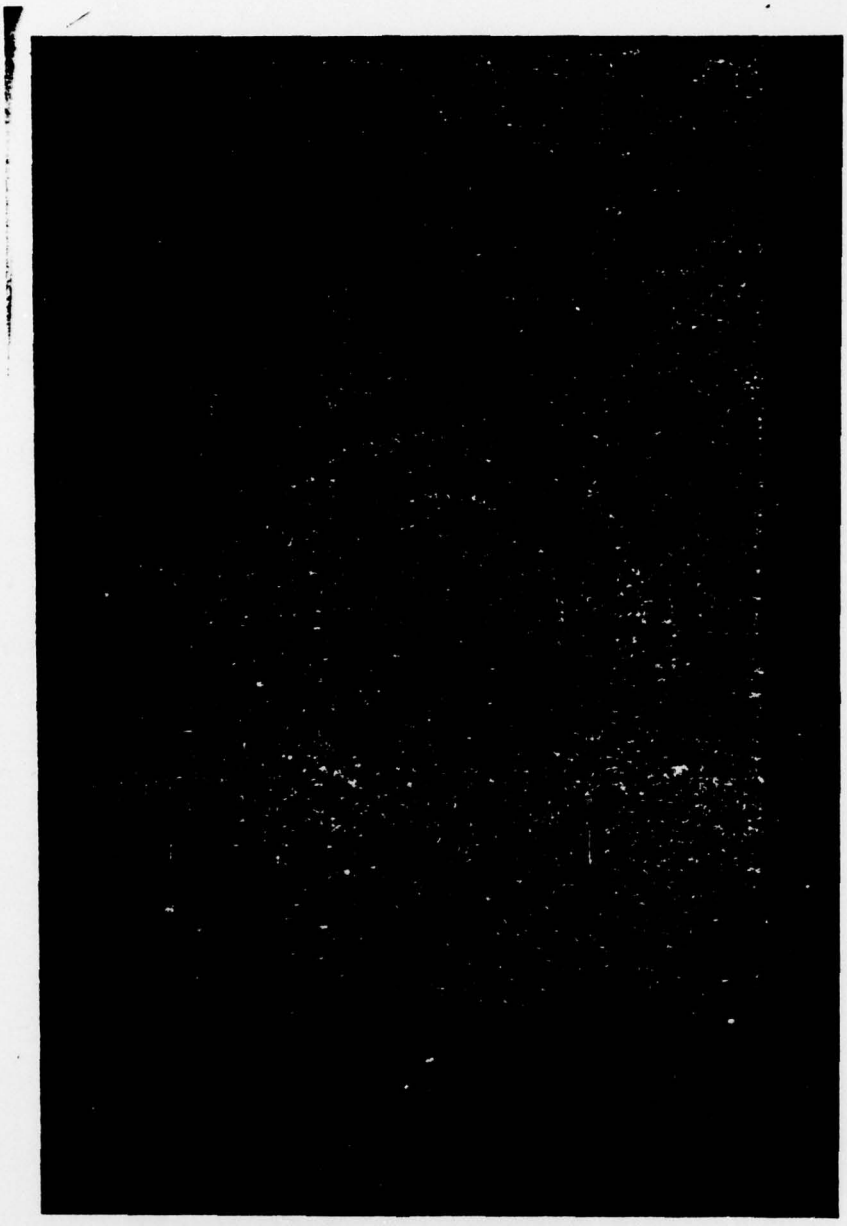

FIGURE 13. Virtual Image of Model 15 μs After Impact at 1767 lb_f Load with .0015 Permanent Strain

TABLE 2. COMPARISON OF RESULTS

EXAMPLE	1	2	3	4	Circle
load, lb_f	880	1767	4420	8835	---
σ_1, psi	1890	3780	9460	18,900	---
ϵ_1, in/in x 10^{-6}	63	1626	315	630	---
major/minor ratio	1.0155	1.0000	1.0419	1.0000	1.0125
corrected ratio	1.0030	.9877	1.0291	.9887	1.0000
theoretical ratio	1.0001	1.0002	1.0004	1.0009	---

IV. RECOMMENDATIONS AND CONCLUSIONS

Straight forward measurement of the major and minor axes of the reconstructed image of the longitudinal wave fronts to obtain the ratio of principal strains is not practical. Notice in all photographs (Figures 11, 12 and 13) that the leading fringe at the top and bottom is not at all distinct, and while the sides are sharper, they still are not well defined. The assumption is that the leading fringe and possibly the second, going radially toward the center of impact, is strictly due to displacements in the plane of the model. This is logical since the holographic arrangement was sensitive to in-plane motion, and the longitudinal wave moves much faster than the transverse wave. Based on all techniques of measurement, assumption and interpretations in this study, wave speed deviation due to elastic strain cannot be accurately measured using dynamic holographic interferometry.

It is recommended that future studies of wave speed deviation due to strain be attempted using ultrasonic techniques. While this change will involve problems and limitations of its own, the primary limitation of accuracy can be overcome [6].

LIST OF REFERENCES

[1] Ranson, W. F., "Use of Holographic Interferometry to Determine the Surface Displacement Components of a Deformed Body," Ph.D. Thesis, Department of Theoretical and Applied Mechanics, University of Illinois, Urbana, Illinois (1971).

[2] Frocht, M. M., Photoelasticity, John Wiley & Sons, Inc., V. I, 1941.

[3] Timoshenko, S., Theory of Elasticity, McGraw-Hill, 1951.

[4] Kolsky, H., Stress Waves in Solids, Dover, 1963.

[5] Hughes, D. S., and Kelly, J. L., "Second-Order Elastic Deformation of Solids," Physical Review, pp. 1145-1149, December 1, 1953.

[6] Egle, D. M., and Bray, D. E., "Measurement of Acoustoelastic and Third Order Constants for Rail Steel," Journal of Acoustic Society of America, V. 60, pp. 741-745, September 1976.

[7] Truesdell, C., "General and Exact Theory of Waves in Finite Elastic Strain," Archive for Rational Mechanics and Analysis, pp. 263-269, 1961.

[8] Turner, J. L., "A Modulated Pulsed Ruby Laser System for Dynamic Holographic Interferometry," M.S. Thesis, Department of Mechanical Engineering, Auburn University, Auburn, Alabama (1972).

APPENDIX A

DYNAMIC HOLOGRAPHIC INTERFEROMETRY

The common method of forming holograms utilizes an off-axis reference beam. Consider the image forming process shown schematically in Figure 14.

In holographic interferometry, two exposures are made of the body. The first exposure is made of the body in some reference configuration. The second exposure is made with the body deformed from the reference configuration. The intensity of the light at the film plane for both exposures [1] can be written

$$I_{FILM} = 2(B^2 + A^2) + ABe^{i(\gamma-\theta)} + ABe^{-i(\gamma-\theta)} + ABe^{-i(\gamma-\theta-\Delta\theta)}$$

where I is the light intensity, A is the amplitude of the object beam, B is the amplitude of the reference beam, γ and θ are phase terms, and $\Delta\theta$ is the phase change due to displacement of the body along a line bisecting the angle α. If α is perpendicular to the surface of the body, then only displacements out of the plane of the body will contribute to fringe formation. If the bisector is not perpendicular to the surface (sometimes called "unequal angle" arrangement) of the body, then displacements in the plane of the body will also contribute to fringe formation. Fringe formation is highly sensitive to displacement of the body. This makes holographic interferometry excellent for

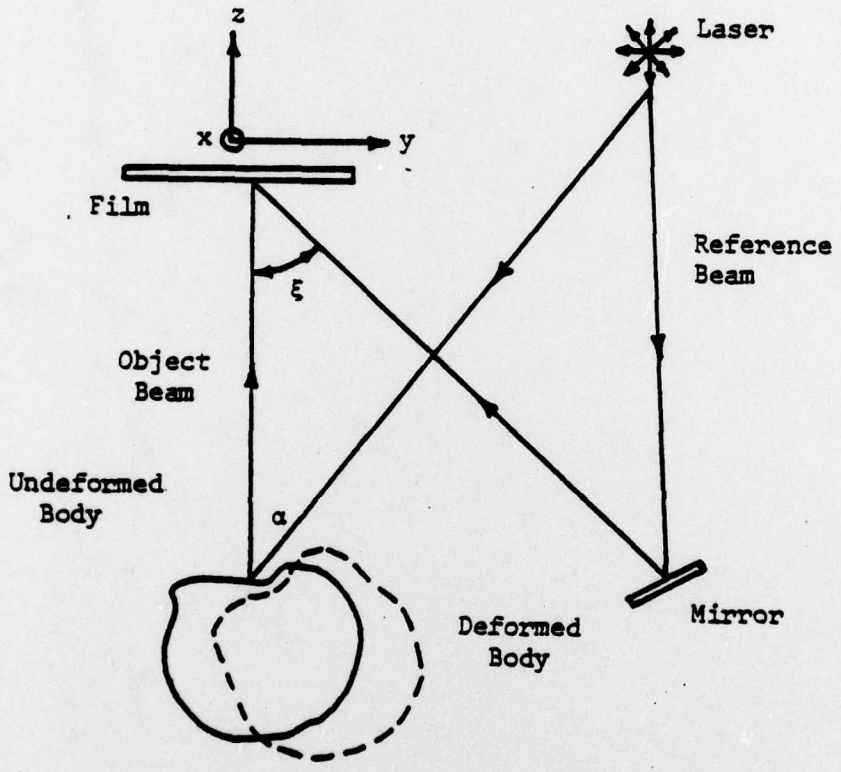

FIGURE 14. An Off-Axis Hologram Configuration For Double-Exposure Holography

studying small displacement phenomenon. The advent of the Q-switched pulsed ruby laser system as a coherent light source for holography has allowed the study of dynamic events. This is possible because of the high intensity and very short duration of ruby pulses.

Reconstruction of the hologram is accomplished by illuminating the film plate with a coherent light source and either viewing the image or projecting the image onto a frosted glass plate as shown in Figure 15.

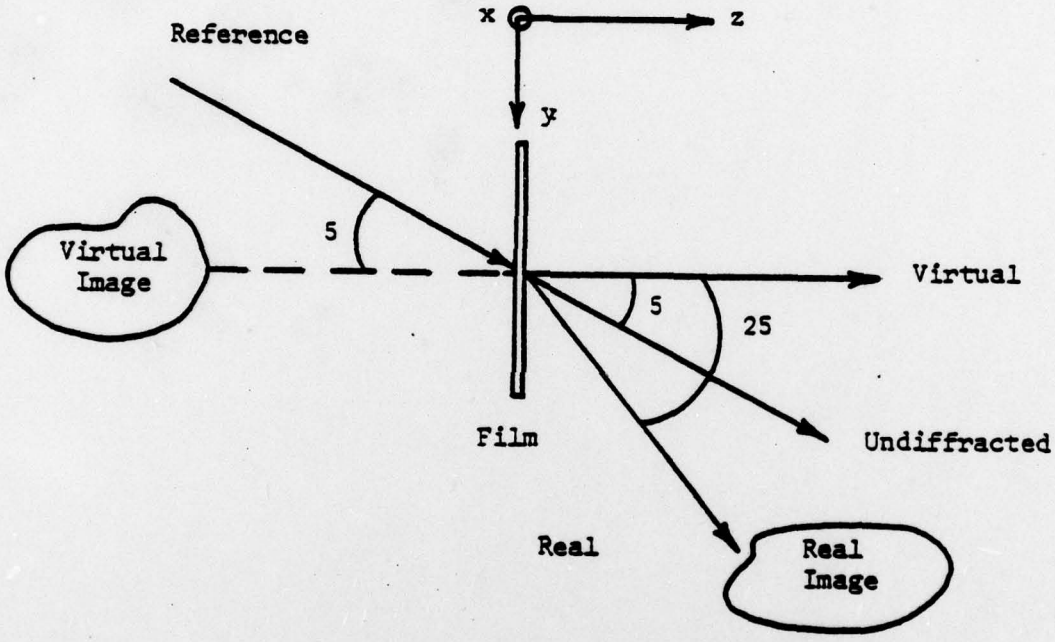

FIGURE 15. Reconstruction of an Off-Axis Reference Hologram

APPENDIX B

EQUIPMENT SETTINGS

Ruby Laser Bench

aperture: .056" diameter

Ruby Lamp Power Supply

capacitor voltage: 1.5 kilovolts

trigger voltage variac: 30%

variac voltage: 71.5 volts

Pulse Generator

pulse width: 1.5 μs

mode: pulse delay

pulse delay time: 15 μs

output pulse amplitude: maximum

Pockels Cell Power Supply

output voltage: 1900 volts

meter reading: 9.5 miliamps

Oscilloscope I

mode: B intensified by A

delay for A: .9 ms

time base A: .2 μs/cm

Oscilloscope I (continued)

time base B: .2 ms/cm

sweep setting: single sweep

coupling B: DC

slope: negative

channel 1 input: 20 volts/cm

channel 2 input: 5 volts/cm

Oscilloscope II

mode: A

time base: 5 μs/cm

sweep setting: single sweep

coupling: AC

slope: negative

input: 2 volts/cm

Air Rifle

bullets undersized: .21"

air pressure: 150 psi